University of Bristol - Explore Bristol Research
General rights

Numerical modelling of 3D woven preform deformations

S.D. Green [a],*, A.C. Long [b], B.S.F. El Said [a] and S.R. Hallett [a]

[a] *Advanced Composites Centre for Innovation and Science (ACCIS), University of Bristol, University Walk, Bristol, BS8 1TR, UK*

[b] *Polymer Composites Research Group, University of Nottingham, University Park, Nottingham, NG7 2RD, UK*

*Corresponding author.E-mail address: steve.green@bristol.ac.uk

ABSTRACT

In order to accurately predict the performance of 3D woven composites, it is necessary that realistic textile geometry is considered, since failure typically initiates at regions of high deformation or resin pockets. This paper presents the development of a finite element model based on the multi-chain digital element technique, as applied to simulate weaving and compaction of an orthogonal 3D woven composite. The model was reduced to the scale of the unit cell facilitating high fidelity results combined with relatively fast analysis times. The results of these simulations are compared with micro computed tomography (CT) scans of a dry specimen of fabric subjected to in-situ compaction. The model accurately depicted all of the key features of the fabric including yarn waviness and cross-sectional shapes as well as their development with compaction. A parametric study is presented to characterise the effect of the model inputs on the analysis speed and accuracy.

Keywords: 3D weave; Textile composites; Finite element analysis (FEA); Preform

1.   Introduction

Composite materials have many desirable properties, most notably excellent stiffness and strength combined with low mass. However, the key disadvantages of traditional 2D composites are that they require expensive, labour intensive manufacturing and are prone to delamination due to the lack of through thickness reinforcement. 3D woven composites can address both of these issues due to the addition of yarns, known as binders, which interlace through the fabric thickness. This means that near net shape preforms can be produced directly from the loom to form composites with greatly improved

interlaminar properties. However, despite these advantages, 3D woven composites have been largely limited to niche applications. One of the key reasons for this is the lack of predictive numerical tools, which limits their ability to be used at the early stages of design.

The literature lists several models to predict the mechanical performance of these materials, with many using idealisation assumptions with respect to the fabric geometry e.g. [1-4]. Such assumptions may include; warp and weft yarns are straight and yarns have a constant cross-sectional shape along length. In reality however, the textile architecture of a 3D woven fabric is very complex, often characterised by significant levels of both in-plane and out-of-plane waviness or crimp, as well as significant changes in cross-sectional shape due to yarn pinching. These characteristics play a significant role in determining the resulting composite performance, especially during damage and failure, where they can lead to strain hardening in tension [5] and kink-band formation in compression [6]. Also, cracks frequently initiate at low strain levels in resin rich regions which form around the binder yarns [7], sometimes even in as-manufactured specimens due to thermal stresses induced from curing [8]. Furthermore, compaction of an as-woven preform to an as-moulded composite causes additional deformations to the textile geometry. Mahadik et al. demonstrated the importance of this effect in an angle interlock 3D woven fabric where the amount of yarn waviness and size and shape of resin pockets varied significantly with the level of compaction [9].

Experimental imaging techniques such as optical microscopy and micro computed tomography (CT) can be used to characterise the internal mesoscopic architecture of textile composite materials. Zhou et al. [10] demonstrated a methodology involving segmentation and reconstruction for using this data to generate geometric models. The key difficulty in such a process is identification of yarn boundaries and Djukic et al. resorted to coating yarns prior to weaving in order to enhance contrast [11]. Any experimental-based method is non-predictive with significant cost and time requirements for each new textile and numerical models to predict fabric deformations have been the subject of considerable interest in recent years. Potluri et al. proposed a finite element (FE) model for fabric compaction consisting of solid continuum elements between rigid plates [12, 13] considering geometric non-linearity and contact with friction. The yarns were assigned transversely isotropic material properties with a relatively low transverse modulus compared to fibre direction modulus and a linear material constitutive law. Lin et al. extended the method by applying a non-linear power law to link pressure and fibre volume fraction (VF)

[14]. These models have the ability to consider the important effects of yarn compaction and bending, as well as friction. As such, they could be used to gain better understanding of the effect of these mechanisms in textile compaction. However, a key limitation is the use solid continuum elements since they do not truly represent the behaviour of a bundle of fibres in a real yarn. Moreover, the initial as-woven geometry used in these models was highly idealised, therefore placing a significant limitation on the accuracy of the final geometry.

The concept of a 'digital element' was introduced by Wang and Sun [15] whereby a yarn is discretised into a chain of 1D rod elements connected by frictionless pins. As the rod length falls towards zero, so does the flexural rigidity of the digital chain so that it possesses only tensile stiffness. In the original approach, the yarn cross-section was considered to be circular and rigid, however, the multi-chain digital element method presented by Zhou et al. [16] extended this method by considering each yarn to be an assembly of several digital chains. Whilst a woven fabric typically comprises of several thousand individual fibres per yarn, 19-69 chains per yarn were used in the study to achieve reasonable analysis times. Inter-yarn contact determined yarn trajectory and intra-yarn contact determined the geometry of the yarn cross-sections, allowing them to take any shape and vary along the yarn length.

Mahadik and Hallett [17] implemented a similar technique in the commercial FE code LS-DYNA, with the key difference being the use of beam elements without a pin connection at the nodes. The yarns therefore possess considerable flexural rigidity and so an elastic-plastic material property was used to assist flexural deformation. Work by Durville [18] described another multi-filament based technique, using an enriched beam element formulation which can account for planar deformations of the cross-sections and allow application of reduced second moment of area properties to prevent inducing a high bending stiffness.

A novel technique was developed by Pickett et al. [19] whereby an initial reference geometry with solid, non-interpenetrating, circular cross-section beams was generated alongside a 'pre-stressed' reference geometry with more realistic elliptical cross-sections attributed to the yarns. The 'initial metric method' in FE code PAM-CRASH was then used to deform the initial mesh towards the reference mesh whilst being bounded by moulding plates and preventing any yarn interpenetration. Stig and Hallström proposed a fundamentally similar technique involving the expansion of yarns, while utilising a slightly different modelling approach [20, 21]. Here, the initial geometry was similar to that used by Pickett et al.

but with yarn surfaces instead meshed with shell elements to form hollow tubes. These yarns were then inflated through the use of hydrostatic fluid elements under general contact conditions until the target yarn volume was achieved.

The work presented in this paper builds on the technique initially developed by Mahadik and Hallett for implementation in a commercial FE code. The model has been reduced to the unit cell scale which has allowed a significant increase in the level of model refinement alongside much reduced analysis times. A technique for applying periodic constraints has been developed since the boundaries of a dry fabric without a resin matrix need special treatment if the output is to give a periodic unit cell for further use in mechanical performance predictions. The modelling process considers not only the effect of weaving but also additional deformations due to compaction during moulding. The results are validated against detailed CT scans at increasing levels of fabric compaction where such additional deformations considerably affected the final fabric configuration. The technique has also been integrated with textile pre-processor TexGen [22] though the use of python scripting for automated model generation. Moreover, a thorough investigation of model input parameters is conducted and used to determine parameter values as well as characterise the effect of each parameter on model results. It is additionally demonstrated that the same parameters identified for the first orthogonal 3D woven fabric investigated can be applied to a different layer-to-layer 3D woven fabric with good results. The model could also be used in the design of 3D woven fabrics to predict the textile features of many different weave styles prior to committing to the time consuming process of setting up the loom for manufacture. This would give designers greater scope to exploit the wide range of textile architectures made possible with 3D weaving technology.

2. Modelling workflow

The workflow of the proposed modelling methodology is illustrated in Fig. 1. Details of steps 1-3 are outlined in the subsequent sections of this paper, while steps 4 and 5 list additional necessary steps required to generate FE models for mechanical performance analysis and are the subject of further publications [23, 24]. The procedure is as follows:

1. An idealised unit cell model of the 3D woven fabric is generated in the textile geometry pre-processor TexGen (Fig. 1a).

2. A python script is used to read the TexGen file and generate and mesh a loosely woven LS-DYNA beam element model with each yarn represented by bundles of chains of beam elements (Fig. 1b). A further script is used to apply boundary conditions in the form of constraint equations.

3. The simulation is conducted, beginning with the loading of yarns to generate an as-woven fabric. Compaction to the target VF is then achieved using rigid plates to produce an as-moulded composite (Fig. 1c).

4. In order to complete the geometrical modelling process the model, consisting of chains of beams, must then be converted to a solid geometry (Fig. 1d). This is done with another user written python script to generate a realistic TexGen model [23].

5. From this model, a FE mesh can be produced (Fig. 1e) for mechanical performance analysis [24], or any other desired analysis for example, resin permeability.

3. Unit cells and boundary conditions

Efficient modelling is based on consideration of the smallest region possible which is representative of a larger structure. Fortunately, the nature of textile composites is that they exhibit a regular, periodic structure. Therefore, an infinite textile can be represented as assembled copies of a unit cell without rotation or reflection [25, 26]. Analysis of a unit cell with the application of appropriate periodic boundary conditions has often been used in the mechanical analysis of 3D woven composites e.g. [1, 3, 4]. One of the key drivers for the deformation modelling presented in this paper is to produce realistic geometry of a 3D textile to be used as an input for such models. However, previous deformation models have used fabric sizes much larger than the unit cell [17, 18]. Compared to a unit cell model, this approach leads to increased analysis time and will place a limit on the level of fidelity that is achievable. Furthermore, without explicitly enforcing the periodicity of the boundary conditions, any edge effects and likely variation though the fabric will make selection of a unit cell, which must be unique and periodic, problematic.

The fabric considered in this study was an orthogonal 3D weave with two sets of binder yarns, each arranged in a 5 harness satin style. One set of these binder yarns float on the upper surface of the

fabric while the other float on the bottom surface. This fabric consisted of 24k warp and weft in-plane yarns and 12k binder yarns to provide through thickness reinforcement, each with 7μm diameter carbon fibres. A schematic representation of this fabric is illustrated in Fig. 2a and Fig. 2b, showing the identified unit cell which has a stagger in tessellation. Periodic constraints were applied to these deformation models purely to enforce periodicity of the unit cell during the analysis. Contrary to the periodic boundary conditions required for mechanical analysis, zero in-plane strain is enforced across the unit cell domain by ensuring that all degrees of freedom remain equal at equivalent nodes at the ends of yarns, as in the following equation and Fig. 2c.

$$u_{i,a} = u_{i,b}, \qquad i = 1,2,3,4,5,6 \tag{1}$$

Where; u_i refers to degree of freedom i and subscripts a and b refer to nodes.

However this alone is not sufficient to enforce periodicity. As the fabric is compacted from its loosely woven state, the yarns flatten and spread from their initial cross-section. Since the binder yarns are in the warp direction, the weft yarns receive some lateral constraint from these yarns to control their deformation. The warp-direction yarns receive lateral constraint from contact with neighbouring parallel yarns. For warp-direction yarns at the unit cell edge, there is no neighbouring yarn with which to contact. Thus these yarns can deform and translate without constraint out of the unit cell as the fabric is compressed. This would ultimately mean that the unit cell is not periodic in the weft direction.

In order to resolve this issue, the unit cell model was extended by one warp-direction yarn at each edge. The constraints described above were still applied to the nodes on the unit cell boundaries to ensure periodicity (Fig. 2c), with the addition of further periodic constraints at the ends of the extended weft yarns, linked to the corresponding points within the unit cell (Fig. 2d). The additional warp-direction yarns were also constrained along their whole length to the corresponding yarns within the unit cell in order to ensure that they deformed appropriately (Fig. 2e). This allows the warp-direction yarns at the edge of the unit cell to come into contact with a neighbouring yarn during deformation and thus be correctly restrained. The application of constraints as described above uses the smallest possible model size to produce a fully periodic unit cell, as demonstrated by the reconstructed TexGen model in Fig. 1d. Other fabrics, depending on design, may require an extension of weft yarns in the same manner.

4. Model setup and inputs

The Python script generates LS-DYNA models by interrogating the idealised TexGen unit cell model in order to extract key parameters of the textile such as yarn spacings in warp and weft, and positions through the fabric thickness. The user can specify the number of beam elements between each cross-over point and the initial cross-section. For a circular cross-sectional shape, the user states the number of concentric layers and the script automatically generates a section with the associated number of beam element chains. The model is expanded to the loosely-woven state to ensure there is no interpenetration of the different yarn cross-sections. For equivalence of the model, the fibre diameter, d_f, and number of fibres per yarn, N_f, from fabric specifications were used to calculate a fibre cross-sectional area for each of the warp, weft and binder yarns. The beam diameters used in the model were hence determined from this area and the number of beam element chains per yarn in the model.

The bending behaviour of yarns is important in textile mechanics and can be assessed experimentally with standard tests such as Kawabata evaluation system (KES-F) [27]. Values of yarn bending stiffness, B, obtained from such tests demonstrate that it is reasonable to neglect the interaction between fibres due to sizing and friction [28]. Thus, yarn bending stiffness can be approximated as the sum of the bending stiffness in the individual fibres, B_f, as in Equation (3).

$$B_f = \frac{E_f d_f^4}{64}$$
(2)

$$B \approx N_f B_f \qquad [28]$$
(3)

Where; E_f is the fibre modulus.

It is not computationally feasible to model a 24k yarn with 24,000 chains of beam elements, thus the discretisation was reduced to 61 chains. Using Equation (3), it can therefore be deduced that such an elastic model of a yarn would lead to a ~400 fold increase in bending stiffness compared to the real yarn. In order to address this, an elastic perfectly plastic material model was used to limit the maximum stress which could be sustained and hence aid flexural deformation of the yarns. This of course has the added effect of allowing the yarns to yield in tension, which is not consistent with real yarn behaviour since the carbon yarns experience negligible longitudinal deformation during processing. However, in the initial

state, the in-plane yarns in the model are nominally straight and the periodic constraints applied to the ends of these yarns prevent any relative displacement. Yarn waviness is often defined as the ratio of the yarn length, l_y, to the projected fabric length, l_f, as in Equation (4).

$$waviness = \frac{l_y}{l_f}$$

(4)

Therefore, for any waviness to form in the model, the yarns must increase from their initial straight length (l_f). Tensile yielding in effect simulates the drawing in of yarns from beyond the unit cell in the real fabric to the new, deformed length (l_y).

The input parameters for the model which gave the most accurate results are listed below, with material properties shown in Table 1.

- **Number of chains per yarn:** 61

- **Initial cross-sectional shape:** Circular

- **Friction:** μ = 0.35

- **Yarn twist rate:** No twist

Note that the material properties are not those of the actual carbon fibre in the fabric. No attempt was made to directly determine inputs based on a mechanical approach by, for example, calibrating the model at the individual yarn level to produce an accurate yarn bending response. The parameters used were instead selected from the parametric study presented in section 8 based on the accuracy of correlation to experimental results and speed of the solution obtained from the model. The model accurately captures the kinematics of the yarn interactions with each other, the tooling and the boundary conditions, but it is not representative of the mechanical forces required to deform and compact the fabric due to the simplifications made in the number of beam element chains per yarn and the yarn contraction method used to achieve the as woven thickness from the initial (but unrealistic) loosely woven configuration.

The model was run on a high performance computing system using eight 2.8 GHz cores taking 8 hours and 55 minutes to complete. Most of the CPU time was due to the significant number of contacts in the model which were handled by a single contact definition.

5. Loading scenario

In order to compact the loosely woven fabric a thermal load in the form of a temperature drop was applied to the binder yarns causing them to contract and hence apply compaction forces to the fabric. A temperature drop of 9.5°C (with a suitably chosen coefficient of thermal expansion of $7.5e^{-2}$ °C^{-1}) was sufficient to bring the fabric to an as-woven thickness of around 7mm. Rigid plates were then gradually brought into contact with the fabric. Compared to experimental observations, it was noted that the binder yarns in the model were relatively tight and so after initial contraction of the fabric, an increase in temperature of 1.0°C was applied to these yarns to better represent the real fabric. During this phase, the plates were held in position at the as-woven thickness of 7mm. The final loading stage in the model was a simulation of the mould closure by applying a prescribed displacement to the plates in order to compact the fabric. The compaction proceeded until a final fabric thickness of 5.5mm, corresponding to a composite VF of 56.25%, was achieved.

6. Experimental methods

Detailed characterisation of the internal fabric architecture through the stages of compaction was conducted with the use of CT scanning. A dry fabric specimen was used since this allowed the fabric to be subjected to an in-situ compaction test, eliminating any effects due to variation between different specimens infused at different thicknesses (as per [9]). This also meant that it was not necessary to infuse multiple samples at the various levels of compaction. A specimen of size approximately 20 unit cells (90 x 55 mm) was cut using a die cutter in a hydraulic press. Such a large size was necessary since cutting and handling the dry fabric inevitably disturbs the yarns at the edges of the specimen. This specimen was housed in an acrylic fixture with bolts in each corner which, when tightened, and in conjunction with use of machined spacers, compacted the fabric to the required thickness (Fig. 3). Four scans were conducted at increasing levels of compaction corresponding to the following composite VFs; 45%, 48.75%, 52.5%, 56.25%.

7.   Model results and validation

   In order to assess and validate the model, results from simulations were compared with CT scans of the real fabric at increasing levels of compaction, see Fig. 4, showing cross-section views of the fabric through the weft yarns. Fig. 5a and Fig. 5b contain further images comparing experimental and model results at a cross-section through the warp yarns and a view of the top surface of the fabric respectively. It can be seen that there is excellent agreement in terms of fabric deformations between the model results and the real fabric in each set of images. The key features noted in these images are described hereafter.

   In the real fabric, the binder yarns are loosely woven with near vertical sections at the crossover points at low levels of compaction (i in Fig. 4a). As the fixture closes, the paths of these yarns alter to become looser still, forming a horse shoe shape. This behaviour is accurately depicted by the model.

   The CT scans show that the stacks of weft yarns adjacent to the binder crossover point (j in Fig. 4d) experience significant horizontal shifting through the fabric thickness. This feature is clearly indicated by the model, although the level of shifting predicted is lower. This shifting is likely to be due to, not only the fabric topology but also to the weaving process, which is not directly simulated in the model. As the binder yarns are tensioned in the model they straighten, applying lateral forces to shift the adjacent weft yarns. However, while doing so, the binder yarns also compact the fabric applying compressive forces which provide frictional resistance to the shifting of these yarns. On the loom, the fabric is not being subjected to the same level of compaction forces and the weft yarns can shift more freely.

   At a low degree of compaction, the experimental images reveal warp yarns with some out-of-plane waviness, though this is at a low level. However, with greater compaction, waviness increases and becomes significant at the highest VF. This waviness is exacerbated by the shifted weft yarns which cause kinking of the warp yarns. The extent of waviness in these yarns and its increase during compaction is very well captured by the model, as is the crimp in the surface weft yarns where they come into contact with the binder yarns (k in Fig. 5a). Yarn waviness is likely to have significant implications for the resulting mechanical properties of the composite, particularly in compression for both strain to failure and strength [6]. With kink band formation noted as a typical damage event, the presence of yarn waviness is clearly an important, if undesirable feature. It is worth noting that in most idealised geometric models, the

warp and weft yarns will be assumed to be straight.

The yarn cross-sectional shapes are also well predicted by the model despite the assumption of an initial circular shape being considerably different from the flatter shapes seen in the final compacted fabric. There are minor differences during compaction as the yarns in the model spread somewhat during compaction whereas the spreading of the real yarns with fabric compaction is more modest. A yarn consisting of several thousand fibres exhibits resistance to spreading due to the friction and entanglement between the fibres as well as the effect of the applied sizing agent. This is not accounted for by the model in which the yarns are represented by a much smaller number of perfectly aligned chains, and as such the yarns in the model have a lower resistance to cross-sectional deformation.

The images of the top view of the fabric demonstrate significant in-plane waviness in the surface weft yarns (l in Fig. 5b) due to the binder yarn style. The model shows very good agreement in this respect and also accurately captures the in-plane crimp of the warp yarns as they divert around the binder yarns at the crossover points (m in Fig. 5b).

8. Parametric study

As part of the development of the modelling technique a variety of input parameters were trialled to arrive at the good correlation with experimental results, as presented previously. In order to formalise and better understand the influence of these different parameters on the results of the model, a parametric study was conducted. Each parameter was varied in isolation using the baseline values stated in section **Error! Reference source not found.**.

8.1. Mass Scaling (convergence study)

In order to achieve reasonable run times for an explicit FE analysis of a quasi-static event it is necessary to scale the density of the model to increase the critical timestep, which is dependent on the speed of sound through the material. The analysis duration is also speeded up compared to the real event, and there are an infinite number of combinations of density and duration which would produce similar results. Density is not a model parameter as such, but it is important that the value used gives a converged

result. An analysis duration of 14s was arbitrarily selected prior to trialling different values of material density (0.2, 0.1, 0.05 and 0.025 tonne/mm^3) until suitably low dynamic effects were noted. The high density models were not adequate since they show a clear difference in the results produced from those with a further reduction in material density. However, reduction of density from 0.05 to 0.025 produced only minor changes in results and it was concluded that a density of 0.05 was sufficient to model the fabric accurately whilst retaining a suitably short analysis time (8hours, 55minutes).

8.2. Number of Chains per Yarn

It is clearly not possible to model each fibre in a yarn as a single chain of beams and computational effort places a practical limit on the number of chains per yarns which is feasible. A previous study featuring a 2D plain weave fabric and a 3D braided fabric suggested that in order to accurately depict the yarn cross-sectional shape 52 chains were required for the former and 19 for the latter [29]. In the case of the orthogonal 3D woven fabric in the study, the yarns are flatter in the as-moulded state then either of those fabrics, such that the cross-section has a larger aspect ratio. The number of chains effectively defines the resolution of the cross-section and a flat section requires more chains per yarn to produce the same resolution along the shortest dimension. Four models were run with 19, 37, 61 and 91 chains per yarn, corresponding to an increase in one concentric layer in the initial circular configuration with each level of refinement. These results are shown in Fig. 6.

It can be seen that the 19 chain model produces poor results with unordered yarn cross-sections which have spread to a single beam thickness in places. The definition of the yarn cross-sectional shape improves with subsequent levels of refinement with the 61 chain model representing the best compromise between analysis time and accuracy of model results. Only very minor improvements are noted with the 91 chain model with a significant computational cost (140% increase). It is suggested that as a guideline yarns should contain at least two to three chains across the thickness in the minimum dimension in their deformed state in order to produce accurate yarn cross-sections. This is achieved in the 61 chain model for this fabric.

8.3. Initial yarn cross-sectional shape

Miao et al. suggested that the selection of initial yarn cross-section did not affect the final fabric configuration in a multi-chain digital element analysis [29]. This study was conducted on a 2D woven fabric using circular and rectangular cross-sections, although the aspect ratio of these shapes was relatively similar. Here, a circular cross-section (aspect ratio = 1) is compared to a flat cross-section (aspect ratio ~2.8) with similar number of chains (59 compared to 61) and corresponding lower initial fabric thickness (see Fig. 7). The outputs from these two models were very similar, with the flat model having a slight reduction in yarn waviness since less deformation was required from the initial state. Despite the flat model having a reduced analysis time, the circular model was selected. This is because it is completely general and avoids making any judgement on the anticipated final yarn shape. Furthermore, it is simple to alter the number of chains per yarn or apply yarn twist, while retaining the same shape.

8.4. Modulus, E

As stated previously, the mechanical properties assigned to the chains were not selected in an attempt to replicate the real properties of the material. It is advantageous to specify a low modulus since this reduces the speed of sound through the material, facilitating faster analysis times. However, in preliminary models with very low values for the modulus, contact issues were encountered since lowering the material stiffness reduces the contact stiffness which can lead to penetrations occurring. Modulus values of 10, 20 and 40 GPa were trialled, with the results of the two extreme models shown in Fig. 8. In each of the models presented here, the contact worked satisfactorily with minimal penetrations. It was also noted that increasing the modulus produces slightly higher levels of crimp and waviness in yarns. However, this effect is small and the modulus does not appear to be a parameter which has a significant effect on model results.

8.5. Yield strength, σ_y

A yield strength of 40 MPa was applied to the binder yarns in all models. This value was found

to offer sufficiently low flexural rigidity while lower values would facilitate excessive tensile yielding during the binder tensioning phase leading to an unpredictable final binder yarn length and hence yarn path. Values of 5, 10 and 20 MPa were trialled for the in-plane yarns and the results of the 5 and 20 MPa models are illustrated in Fig. 9. As expected, the yield strength has an important effect of the formation of waviness in the in-plane yarns, with lower values encouraging greater waviness as the yarns can extend and deform more easily.

8.6. Friction, μ

The effect of friction is known to be an important parameter in textile mechanics, affecting how a fabric deforms during processing [30]. Friction occurs both between fibres within a yarn and between yarns themselves with energy dissipation due to friction being the cause of permanent deformation within the fabric. A co-efficient of friction of 0.35 was selected for the model on the basis of the quality of results that were produced. In this parametric study values of 0.2 and 0.6125 were also trialled, with the results of these two models shown in Fig. 10.

These images show significant differences between the models, confirming that friction has an important effect on the results. Yarn spreading was reduced in the high friction model due to an increase in resistance to cross-sectional deformation caused by greater intra-yarn friction. As such, friction could be used as a means of compensating for the low resistance to cross-sectional deformation in the model. However, applying a high level of friction globally to the model also produces greater inter-yarn friction which, in conjunction with reduction in yarn spreading, has led to an increase in yarn waviness. Note that these effects are related since the high level of crimp allows pockets to form around the yarns helping them retain their shape.

8.7. Twist

In a separate attempt to control yarn spreading, a model with twisted yarns was generated since twisted yarns have a greater resistance to cross-sectional deformation than straight yarns [31]. Compared to using a high level of friction, twisted yarns allows direct control of intra-yarn deformation without

affecting inter-yarn behaviour. A low level of twist of ~3 °/mm was applied to this model, corresponding to less than 90° of yarn rotation along the largest dimension of the unit cell. The addition of twist was found to increase yarn waviness as the in-plane yarns would yield in tension at the expense of yarn spreading. Therefore, in order to create a twisted model that produced similar levels of crimp as the untwisted model, the yield strength was increased from 10 to 20 MPa. The results of these models are compared in Fig. 11.

It is evident that similar levels of waviness are indeed produced by both models, although there are some differences in the predicted yarn cross-sectional shapes. Overall, yarn spreading remains similar in the two models, however, the level of yarn spreading in the twisted model is consistent through the thickness, as well as during compaction. Conversely, in the untwisted model the yarns in the centre of the fabric spread notably more than those on the surface, especially at high levels of compaction.

Untwisted yarns were used in the final model since the differences between the models were not considered significant, and the addition of twisted yarns would mean an extra input parameter to the model. However, the use of twisted yarns could be an option to control yarn cross-sectional deformation if deemed necessary for a particular fabric.

9. Application to a different fabric

Whilst the model required calibration in the first instance in order to produce results with a close match to experimental data, the aim is for it to be able to simulate many types of fabric. In order to test this, the same input parameters were blindly applied to a substantially different layer-to-layer 3D woven fabric. Model predictions are compared against subsequent CT scan images at two levels of compaction, corresponding to VFs of 32.3% (as-woven) and 39.0%, in Fig. 12. Very good results are produced by the model in terms of yarn cross-sections and waviness at both levels of compaction.

10. Discussion and conclusions

A textile deformation model, representing each yarn by 61 chains of beam elements has been developed and applied to model an orthogonal 3D woven fabric at the unit cell level. Comparison of the

15

model results and experimental images showed very good agreement. Each of the textile features, and the significant further deformations with compaction, were well represented by the model, thus validating its accuracy. The specific fabric used in this study was particularly difficult to model due to the complex internal architecture featuring weft yarn shifting and significant levels of both in-plane and out-of-plane waviness in the warp and weft yarns caused by the style of binder yarns. Further work [24] has shown that mechanical FE models of this fabric using idealised geometry significantly overestimated stiffness and strength whereas the realistic geometry produced from the simulations detailed in this paper gave a much closer match with experimental data. This clearly demonstrates the need for a model to predict realistic textile geometry when considering textile composite with complex internal architecture.

The objective of the proposed model was to be completely general in applicability, able to simulate a wide range of fabrics. A parametric study showed model results to be independent of yarn initial cross-sectional shape and material modulus. The number of chains per yarn had an effect on the resolution and accuracy of yarn cross-sectional shapes, with 61 chains being able to produce detailed results with reasonable analysis times. This number of chains should also be sufficient for most other fabric types since the final yarn shapes for this fabric had a high aspect ratio. Varying the friction coefficient or yield strength had consequences on the results. However, only a narrow range of variation in final results was noted and the effects were similar for both parameters with the level of waviness in the warp and weft yarns being altered. Application of the same parameters as determined through the parametric study were shown to produce good results when applied to a significantly different 3D woven fabric type, thus demonstrating the wider applicability of the model. Nonetheless, there are various machine parameters used during weaving, in addition to fabric topology, which affect yarn waviness and may limit the range of fabric types and examples over which one set of parameters can be used. Beyond this, slight recalibration may be required in order to produce the highest quality results by using the yield strength as a sole calibration parameter to directly control the level of waviness.

11. Acknowledgements

References

[1]   Crookston JJ, Kari S, Warrior NA, Jones IA, Long AC. 3D textile composite mechanical properties prediction using automated FEA of the unit cell. ICCM-16. Kyoto, July, 2007.

[2]   Lee CS, Chung SW, Shin H, Kim SJ. Virtual Material Characterization of 3D Orthogonal Woven Composite Materials by Large-scale Computing. Journal of Composite Materials. 2005;39:851-63.

[3]   Wang XF, Wang XW, Zhou GM, Zhou CW. Multi-scale Analyses of 3D Woven Composite Based On Periodicity Boundary Conditions. Journal of Composite Materials. 2007;41:1773-88.

[4]   Biragoni P, Hallett S. Finite element modelling of 3D woven composites for stiffness prediction. ICCM-17. Edinburgh, July, 2009.

[5]   Cox BN, Dadkhah MS, Morris WL. On the tensile failure of 3D woven composites. Composites Part A: Applied Science and Manufacturing. 1996;27:447-58.

[6]   Mahadik Y, Hallett SR. Effect of fabric compaction and yarn waviness on 3D woven composite compressive properties. Composites Part A: Applied Science and Manufacturing. 2011;42:1592-600.

[7]   Callus PJ, Mouritz AP, Bannister MK, Leong KH. Tensile properties and failure mechanisms of 3D woven GRP composites. Composites Part A: Applied Science and Manufacturing. 1999;30:1277-87.

[8]   Tsukrov I, Bayraktar H, Giovinazzo M, Goering J, Gross T, Fruscello M, et al. Finite Element Modeling to Predict Cure-Induced Microcracking in Three-Dimensional Woven Composites. International journal of fracture. 2012:1-8.

[9]   Mahadik Y, Brown KAR, Hallett SR. Characterisation of 3D woven composite internal architecture and effect of compaction. Composites Part A: Applied Science and Manufacturing. 2010;41:872-80.

[10] Zhou E, Mollenhauer D, Iarve E. Image reconstruction based modeling of 3D textile composites. 48th AIAA/ASME/ASCE/AHS/ASC Structures, Structural Dynamics, and Materials Conference. Honolulu 2007.

[11] Djukic LP, Herszberg I, Walsh WR, Schoeppner GA, Gangadhara Prusty B, Kelly DW. Contrast

enhancement in visualisation of woven composite tow architecture using a MicroCT Scanner. Part 1: Fabric coating and resin additives. Composites Part A: Applied Science and Manufacturing. 2009;40:553-65.

[12] Potluri P, Sagar TV. Compaction modelling of textile preforms for composite structures. Composite Structures. 2008;86:177-85.

[13] Potluri P, Long A, Young RJ, Lin H, Shyng Y-T, Manan A. Compliance modelling of 3D weaves. ICCM-16. Kyoto, July, 2007.

[14] Lin H, Sherburn M, Crookston J, Long AC, Clifford MJ, Jones IA. Finite element modelling of fabric compression. Modelling and Simulation in Materials Science and Engineering. 2008;16:035010.

[15] Wang Y, Sun X. Digital-element simulation of textile processes. Composites Science and Technology. 2001;61:311-9.

[16] Zhou GM, Sun XJ, Wang YQ. Multi-chain digital element analysis in textile mechanics. Composites Science and Technology. 2004;64:239-44.

[17] Mahadik Y, Hallett SR. Finite element modelling of tow geometry in 3D woven fabrics. Composites Part A: Applied Science and Manufacturing. 2010;41:1192-200.

[18] Durville D. Simulation of the mechanical behaviour of woven fabrics at the scale of fibers. International Journal of Material Forming. 2010;3:1241-51.

[19] Pickett AK, Sirtautas J, Erber A. Braiding simulation and prediction of mechanical properties. Applied Composite Materials. 2009;16:345-64.

[20] Stig F, Hallström S. Spatial modelling of 3D-woven textiles. Composite Structures. 2012;94:1495-502.

[21] Stig F, Hallström S. A modelling framework for composites containing 3D reinforcement. Composite Structures. 2012.

[22] Sherburn M. Geometric and mechanical modelling of textiles [PhD thesis]: University of Nottingham, 2007.

[23] Green SD, Long AC, Hallett SR. Simulated textile geometry with realistic deformations for finite element modelling. TexComp-11. Leuven, September, 2013.

[24] Green SD, Matveev MY, Long AC, Hallett SR. Modelling of 3D woven composites with realistic

unit cell geometry. ICCM-19. Montreal, July, 2013.

[25] Tang X, Whitcomb JD. General techniques for exploiting periodicity and symmetries in micromechanics analysis of textile composites. Journal of Composite Materials. 2003;37:1167-89.

[26] Li S, Warrior N, Zou Z, Almaskari F. A unit cell for FE analysis of materials with the microstructure of a staggered pattern. Composites Part A: Applied Science and Manufacturing. 2011;42:801-11.

[27] Kawabata S. The Standardization and Analysis of Hand Evaluation. 2 ed. Osaka: The Textile Machinery Society, 1980.

[28] Long AC. Design and Manufacture of Textile Composites. Cambridge: Woodhead Publishing, 2005.

[29] Miao Y, Zhou E, Wang Y, Cheeseman BA. Mechanics of textile composites: Micro-geometry. Composites Science and Technology. 2008;68:1671-8.

[30] Somashekar A, Bickerton S, Bhattacharyya D. An experimental investigation of non-elastic deformation of fibrous reinforcements in composites manufacturing. Composites Part A: Applied Science and Manufacturing. 2006;37:858-67.

[31] Naik N, Kuchibhotla R. Analytical study of strength and failure behaviour of plain weave fabric composites made of twisted yarns. Composites Part A: Applied Science and Manufacturing. 2002;33:697-708.
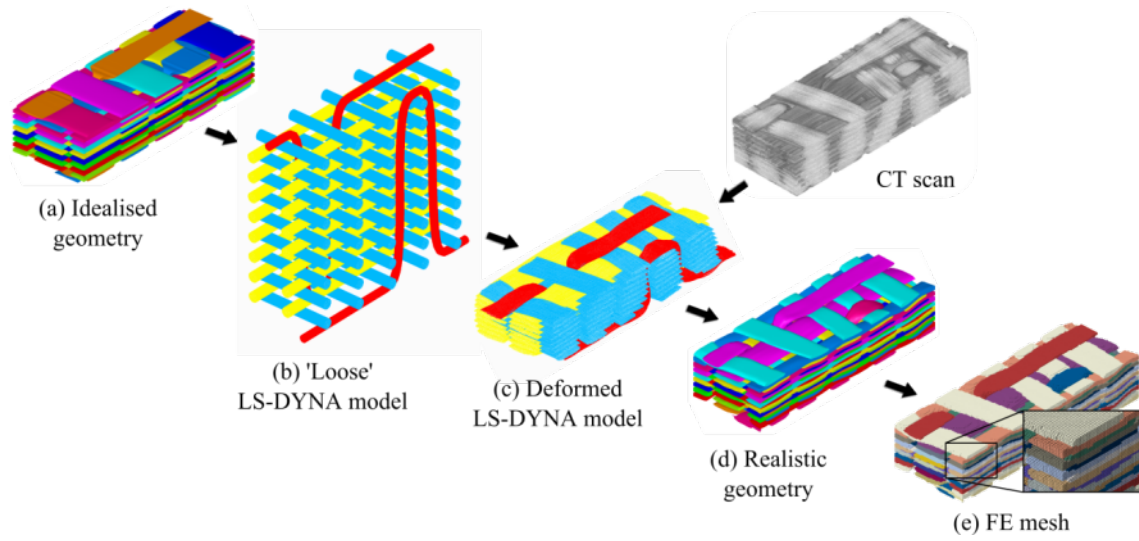
Figure Captions

Fig. 1. Overview of workflow in the modelling process, showing validation with CT scan.
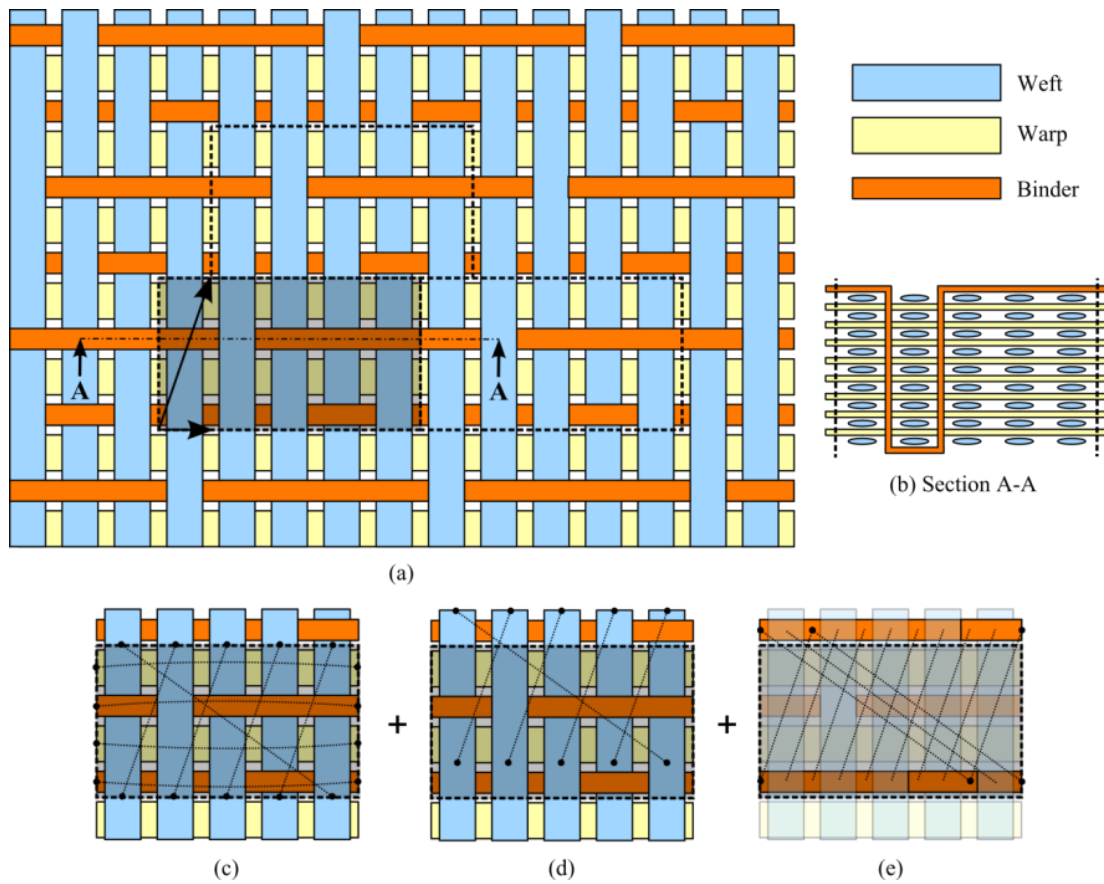
Fig. 2. Schematic of fabric showing; (a) plan view with tessellation of unit cell, (b) section view, application of periodic boundary conditions to extended unit cell model for; (c) inner unit cell, (d) extended weft yarns, (e) extended warp-direction yarn.

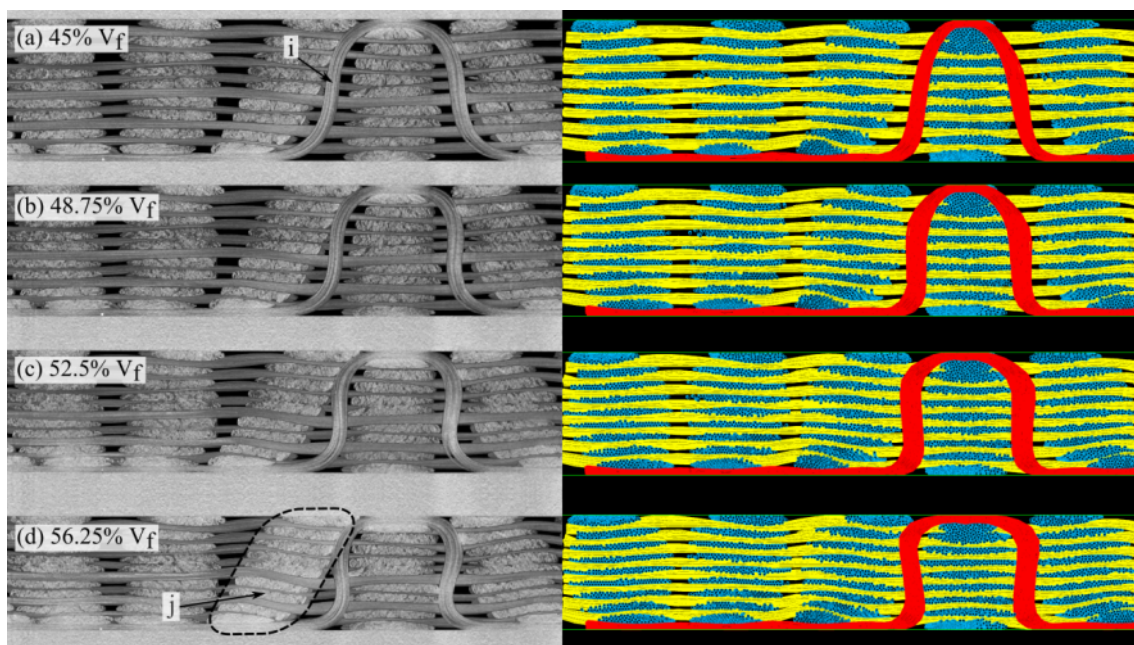**Fig. 3.** Dry fabric specimen in acrylic fixture.

Fig. 4. CT scan images and model results showing cross-section view of fabric through the weft yarns (section A-A in Fig. 2a) at increasing levels of compaction.
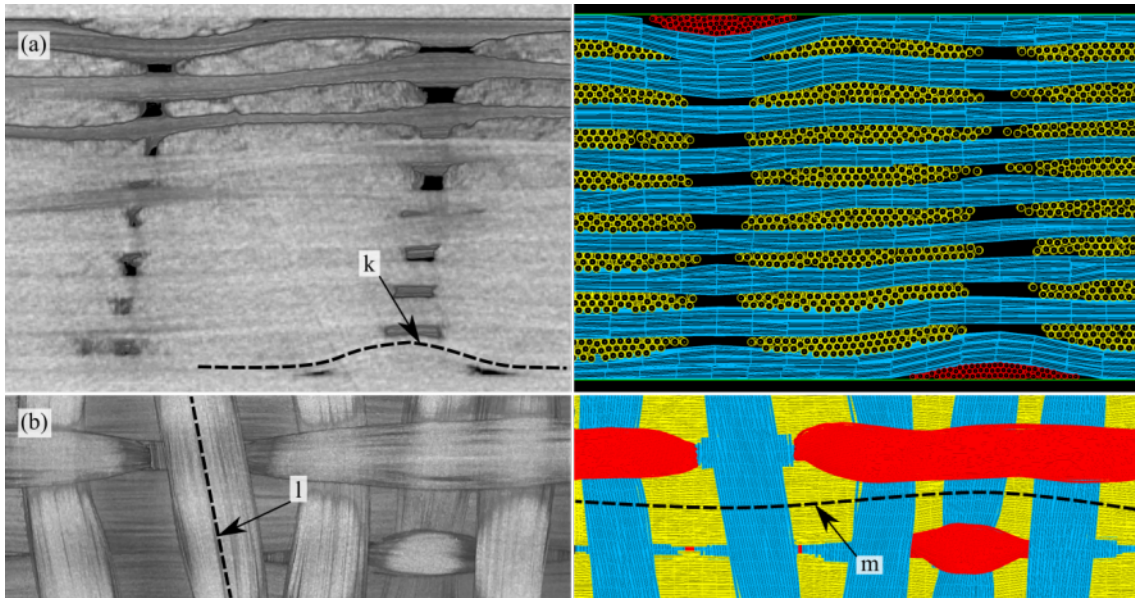
Fig. 5. CT scan images and model results at 52.5% VF showing fabric; (a) cross-section view through warp yarns (section B-B in Fig. 2a), (b) top surface.
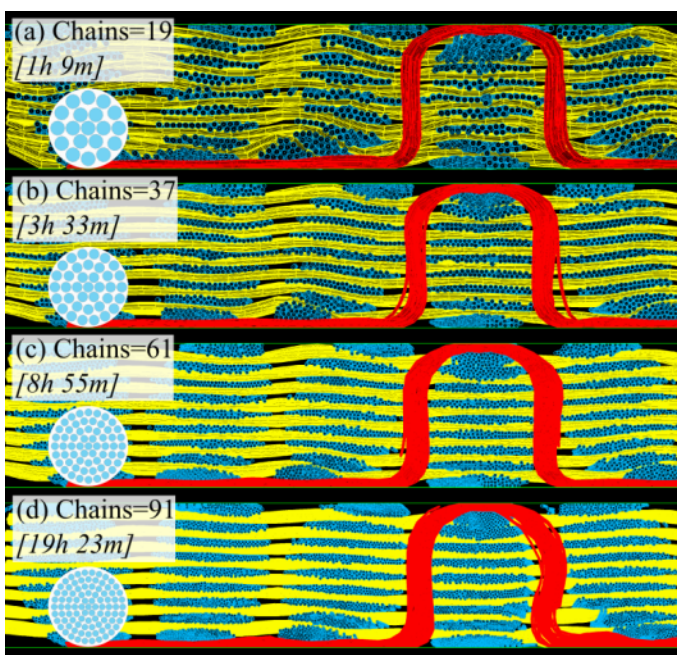
Fig. 6. Model results at 52.5% VF with increasing numbers of chains per yarn, showing initial circular configuration of a weft yarn.

Fig. 7. Initial and final configurations (52.5% VF) of; (a) circular cross-section model, (b) flat cross-section model.

Fig. 8. Model results at 52.5% VF with low and high moduli.

Fig. 9. Model results at 52.5% VF with low and high yield strength.

Fig. 10. Model results at 52.5% VF with low and high friction.

Fig. 11. Model results at 52.5% VF with untwisted and twisted yarns.

Fig. 12. CT scan images and model results for layer-to-layer fabric showing; (a) low compaction, (b) high compaction.

Fig. 13. Overview of workflow in the modelling process, showing validation with CT scan.

Fig. 14. Schematic of fabric showing; (a) plan view with tessellation of unit cell, (b) section view,

application of periodic boundary conditions to extended unit cell model for; (c) inner unit cell, (d)

extended weft yarns, (e) extended warp-direction yarn.

Fig. 15. Dry fabric specimen in acrylic fixture.

Fig. 16. CT scan images and model results showing cross-section view of fabric through the weft yarns (section A-A in Fig. 2a) at increasing levels of compaction.

Fig. 17. CT scan images and model results at 52.5% VF showing fabric; (a) cross-section view through warp yarns, (b) top surface.

Fig. 18. Model results at 52.5% VF with increasing numbers of chains per yarn, showing initial circular configuration of a weft yarn. (For interpretation of the references to colour in this figure legend, the reader is referred to the web version of this article.)
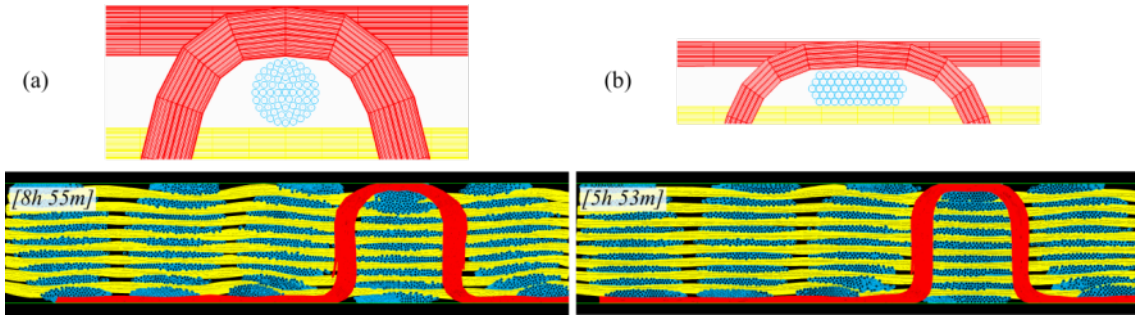
Fig. 19. Initial and final configurations (52.5% VF) of; (a) circular cross-section model, (b) flat cross-section model. (For interpretation of the references to colour in this figure legend, the reader is referred to the web version of this article.)
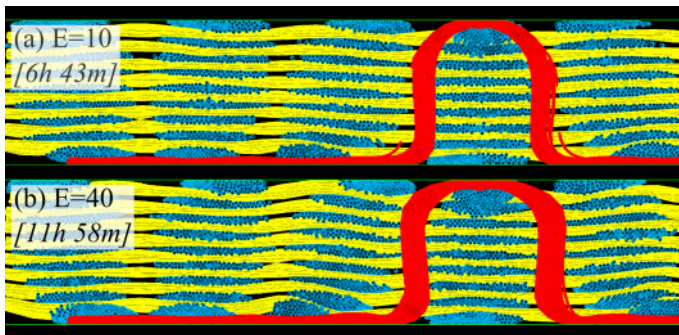

Fig. 20. Model results at 52.5% VF with low and high moduli. (For interpretation of the references to colour in this figure legend, the reader is referred to the web version of this article.)
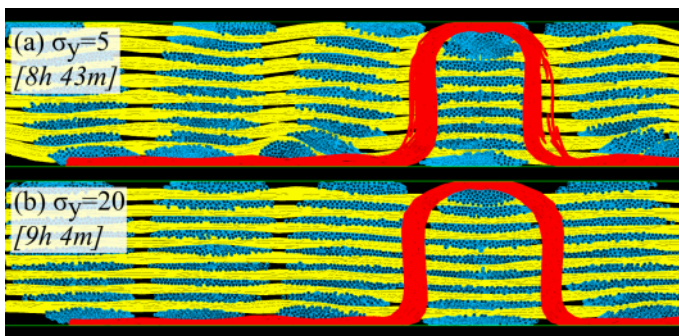

Fig. 21. Model results at 52.5% VF with low and high yield strength. (For interpretation of the references to colour in this figure legend, the reader is referred to the web version of this article.)
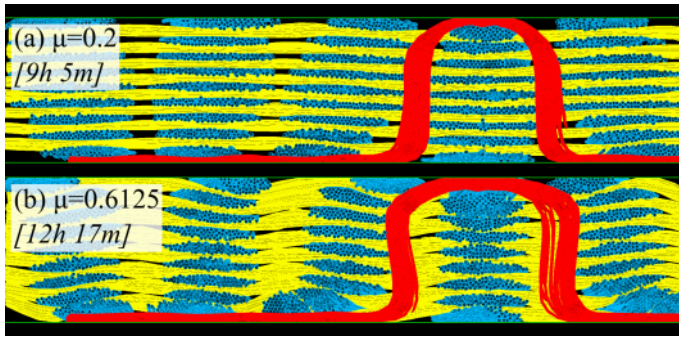
Fig. 22. Model results at 52.5% VF with low and high friction. (For interpretation of the references to colour in this figure legend, the reader is referred to the web version of this article.)
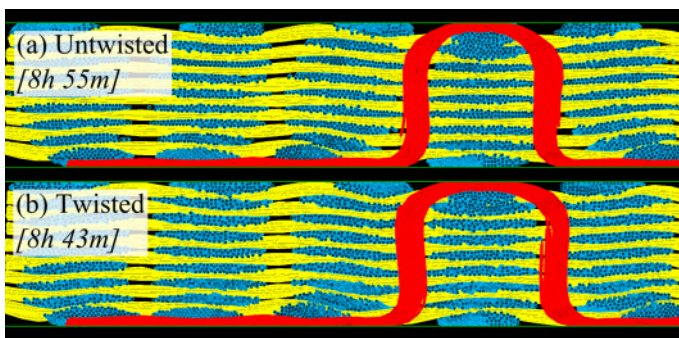

Fig. 23. Model results at 52.5% VF with untwisted and twisted yarns. (For interpretation of the references to colour in this figure legend, the reader is referred to the web version of this article.)
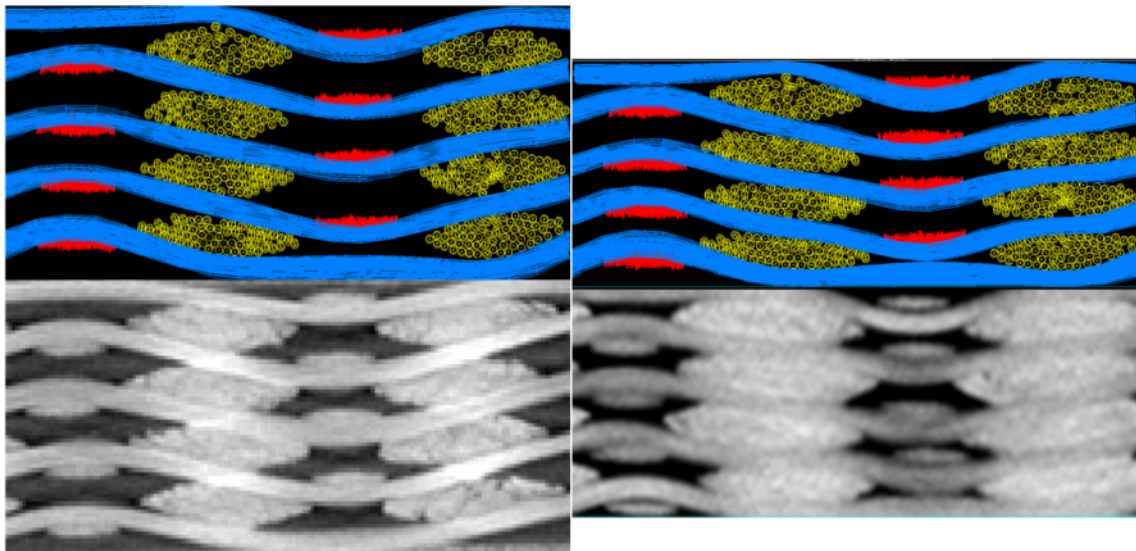

Fig. 24. CT scan images and model results for layer-to-layer fabric showing; (a) low compaction, (b) high compaction. (For interpretation of the references to colour in this figure legend, the reader is referred to the web version of this article.)

Tables

Table 1 Material properties applied to yarns in model compared with carbon fibre.

	Binder yarns	Warp / weft yarns	Carbon fibre
ρ (tonne/mm3)	0.05	0.05	1.75e-9
E (GPa)	20	20	230
σ_y (MPa)	40	10	3400